Jordan Journal of Civil Engineering, Volume **18**, No. **4**, **2024**
DOI: https://doi.org/10.14525/JJCE.v18i4.11

Jordan Journal of Civil Engineering

Journal homepage: https://jjce.just.edu.jo

Numerical Modeling of Structural Steel Elements Fabricated Using Wire and Arc Additive Manufacturing

Nada Mamdouh [1)], ***Yasser N. Saleh*** [1)], ***Amr M. Ibrahim*** [1)*]

[1)] *The British University in Egypt, Civil Engineering Department, El Shorouk, Egypt.*
** Corresponding Author. E-Mail: amr.ibrahim@bue.edu.eg*

ARTICLE INFO

Article History:
Received: 8/7/2024
Accepted: 29/9/2024

ABSTRACT

Additive manufacturing (AM) has revolutionized numerous industrial fields by enabling the production of intricate shapes that were previously impractical to manufacture using traditional methods. Recently, AM has been adopted in the construction industry. One of the key challenges in researching additively manufactured (AM'd) parts is accurately modeling and analyzing their thermal and mechanical responses and considering the imperfections resulting from the temperature variation during the printing process. This requires a comprehensive understanding of the interplay between various parameters, such as the printing process, and material properties. Overcoming these challenges is crucial for improving the reliability and performance of AM'd parts. Consequently, this research provides a step-by-step modeling and simulation of AM'd parts using ABAQUS software. Specimens with different test setups and printing directions were used for simulation. Four simulations had been created for specimens using layer-by-layer method to represent the 3D printing process fabricated using wire and arc additive manufacturing (WAAM). Also, finite element modeling was performed to investigate the specimen response under the application of tension and compression loads. This research provided insights into the differences in modeling the mechanical properties relative to the printing directions and where the tensile and compressive capacities were greatly influenced.

Keywords: WAAM, Tensile testing, Finite element analysis, Stainless steel.

INTRODUCTION

The development of engineering structures requires a significant amount of material consumption, while traditional construction techniques often result in a significant amount of material waste. Additive manufacturing (AM), or 3D printing, is developed to replace traditional construction techniques, where an object is created by adding successive layers (Guo & Leu, 2013; Megahed et al., 2016). AM technology relies on producing exact 3D objects without wasting materials during the manufacturing process. AM has been applied in diverse fields, such as biomedical engineering, structural engineering, and aerospace due to its efficiency. Also, it allows designers to create geometrically complex parts from different materials (Calignano et al., 2017; Singh et al., 2017; Sequeira Almeida, 2012).

AM technology has a variety of printing processes that could be categorized according to their heat sources and feedstock material (van Bolderen, 2017). AM processes could be powder bed processes, powder fed processes, or wire feed processes, as illustrated in Fig. (1) (Rosli et al., 2021). In this research, wire and arc additive manufacturing (WAAM) technology will be considered, as it is the most widely used technology in structural engineering applications due to its high deposition rate and availability to be applied for manufacturing medium and large components (Laghi et al., 2021).

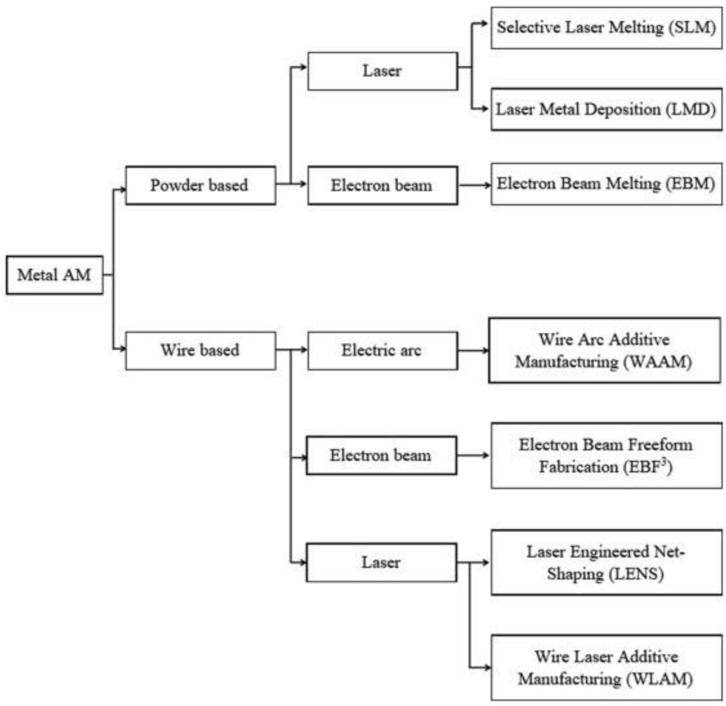

Figure (1): Metal AM processes (Rosli et al., 2021)

WAAM could be performed through various techniques, such as continuous, layer-by-layer, printing (Gardner et al., 2020; Feucht et al., 2019; Feucht et al., 2020) or dot-by-dot printing methods (Kloft et al., 2020; Mechtcherine et al., 2021; Müller et al., 2019). The continuous method is producing an object through printing successive continuous layers. However, the dot-by-dot method is creating the object by printing separated points which could be at different layers. Choosing either method will affect the strength and the mechanical properties of the printed specimen (Laghi, 2021).

Additively manufactured elements are subjected to several drawbacks which affect the elements' mechanical properties. Those drawbacks are mainly caused by geometric imperfections and changes of printing angles (Laghi et al., 2022). Most geometric imperfections are in the variation of layer thicknesses and surface irregularities along the specimen due to the exposure to high temperature in the printing process (Feucht et al., 2019; Kraus et al., 2022; Laghi et al., 2020a). Thus, further post-processing is needed to smooth the surfaces (Kyvelou et al., 2020).

Extensive research has investigated the structural behavior of the AM'd components in order to ensure their capability of withstanding heavy loads without excessive deformation, damage, and changes in the mechanical properties (Laghi et al., 2020b). Various tests have been performed on different specimens to study their behavior in tension (Laghi et al., 2022; Laghi et al., 2020a; Kyvelou et al., 2020; Kořínek et al., 2021), compression (Zhang et al., 2021; Zhang et al., 2023), and fatigue (Huang et al., 2023; Ayan and Kahraman, 2022). Van Bolderen (2017) and Huang et al. (2022a) investigated load-carrying capacity of the AM'd elements in flexure as well as the influence of printing imperfections *via* 4-point bending tests. The difference in behavior between machined and unmachined printed specimens has been also investigated (Laghi et al., 2020a; Kyvelou et al., 2020; Silvestru et al., 2022). From these previous studies, it was observed that using different printing techniques with different printing angles affects the specimens' mechanical properties. This anisotropic mechanical property coupled with the geometric imperfections set a challenge for numerical modeling of AM'ed elements (Hadjipantelis et al., 2022).

In the experimental and numerical study conducted by Silverstru et al. (2022), tensile and compressive loads were applied to test specimens. They simulated each 3D printed specimen as one part using ABAQUS. For the tension test, the results obtained showed a similar trend for all specimens in their elastic behavior and yield plateau level. However, necking of the coupon specimens took place at different displacement values in the experiment than that extracted from the numerical models. Despite the results, ductility requirements according to Eurocode have been met by the experimental results. For the compression test, the authors investigated a series of 3D printed bars. The finite element model (FEM) results showed that there was a deviation between experimental and FEM curves. The FEM has behaved more stiffer than the experimental testing and did not achieve the same behavior. However, it could be used to detect the maximum reached force.

Zhang et al. (2021) developed a FEM of a circular hollow section (CHS) column to compare the simulation results with the experimental results recorded. The FEM stress values were not affected by changing the imperfection amplitude which demonstrated the insensitivity of the CHS column to local imperfections. However, the imperfection amplitude affected the deformations at ultimate stresses. The failure mode of the FEM was close to the test failure mode, as shown in Fig. (2).

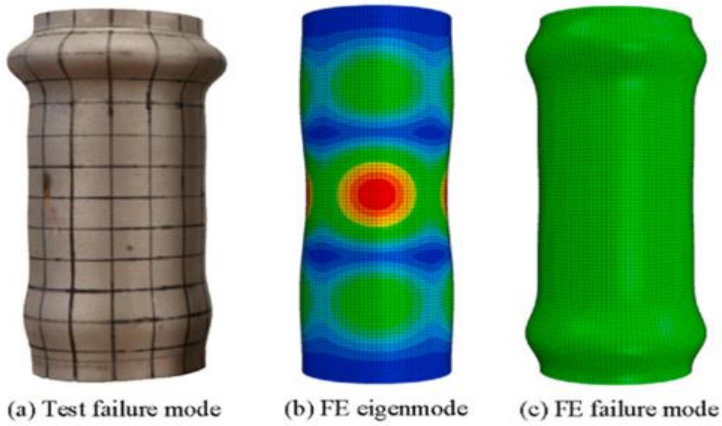

Figure (2): Compression failure modes of the CHS column from (a) the experimental testing, (b) finite element eigenmode, and (c) finite element failure mode (Zhang et al., 2021)

Korinek et al. (2021) investigated the mechanical behavior of AM'd specimens both experimentally through tension and torsion tests, and numerically. The study used von-Mises yield criterion and Hill yield criterion to simulate the material properties. It was significant to define either criterion, as changing printing direction influenced the specimen's mechanical response. The results from numerical modeling indicated that simulation using Hill criterion had a more accurate and better description of yielding than using von-Mises criterion.

FE simulations are commonly employed to examine the behavior of structural elements, significantly reducing the need for extensive experimental work. In the WAAM process, the final geometry is achieved by layering molten weld metal, which often results in substantial residual stresses and distortions in the produced parts. Numerical simulations can estimate these residual stresses occurring during and after the printing process using thermo-mechanical models; however, achieving high accuracy is associated with considerable computational expense (Ding et al., 2011; Chiumenti et al., 2010). Ding et al. (2011) analyzed the effectiveness of steady-state thermo-mechanical models in reducing computation time compared to transient models. They also compared the Eulerian reference frame with the Lagrangian approach, utilizing 8-node linear brick elements (DC3D8) for thermal simulation in the Lagrangian model. ABAQUS software was used for the FE analysis, with a DFLUX user subroutine implemented to simulate the moving heat source based on the double ellipsoidal heat source. The element birth technique was also employed, where all elements except the substrate base plate are initially deactivated, and then progressively reactivated using the *Model Change option in ABAQUS's interaction module. It was concluded that the steady-state approach could reduce computational time by up to 80%; however, both the transient and steady-state simulations had high computational cost. Stress redistribution was noted after the substrate base layer was unclamped.

Xiong et al. (2017) explored the impact of preheating the substrate to reduce thermal stress issues, using a transient heat transfer model that was experimentally validated. They adopted the double ellipsoid heat source model for simulating heat flux during the deposition process, combined with the element birth and death technique. Their numerical model demonstrated good correlation with experimental results, with a deviation range from 5% to 20%, which was attributed to factors, such as constant heat source parameters and the omission of heat conduction modeling between the substrate and the platform. Abusalma et al. (2022) investigated the optimization of process parameters to minimize residual stresses in WAAM-fabricated parts. Their research involved experimentally validated numerical models that examined the effects of torch travel speed and interlayer dwell time on residual stress development. The study tested three travel speeds (6 mm/s, 9 mm/s, and 11 mm/s) and found that these speeds had minimal impact on stress distribution along the build direction. Additionally, three different dwell times (50 s, 1 min, and 2 min) were evaluated. Longer dwell times resulted in a shallower region of high tensile stress at the top of the wall compared to shorter dwell times. Shorter dwell times maintained higher temperatures in more layers, leading to shrinkage and tensile stress formation upon cooling. The research concluded that shorter dwell times produced more uniform stress profiles.

WAAM technology can be a significantly useful approach for manufacturing optimized steel sections that are deemed difficult to achieve using conventional approaches (Saleh et al., 2024; Barakat et al. 2022; Galeb & Khayoon, 2013). Therefore, it is crucial to understand the anisotropic nature of WAAM parts and how to model them numerically. In line with the current research efforts on finite element (FE) modeling of AM'd elements, this paper introduces a novel modeling technique designed to capture the structural behavior of additively manufactured structural members using simplified thermo-mechanical models. ABAQUS software (2019) was used for the numerical simulation. to produce layer-by-layer simulation for 3D printing in tension and compression, taking into consideration the temperature changes and geometric imperfections of the elements.

PROPOSED NUMERICAL APPROACH

3D finite element numerical simulations have been created for AM'd dog-bone specimens and verified against the tensile test results by Kyvelou et al. (2020) in three different directions relative to the direction of printing, as illustrated in Fig. 3 (a), and tested in tension. In addition, numerical simulation for compression testing presented by Huang et al. (2022b) on CHS column has been created to investigate the variations between the tension simulation and the compression simulation.

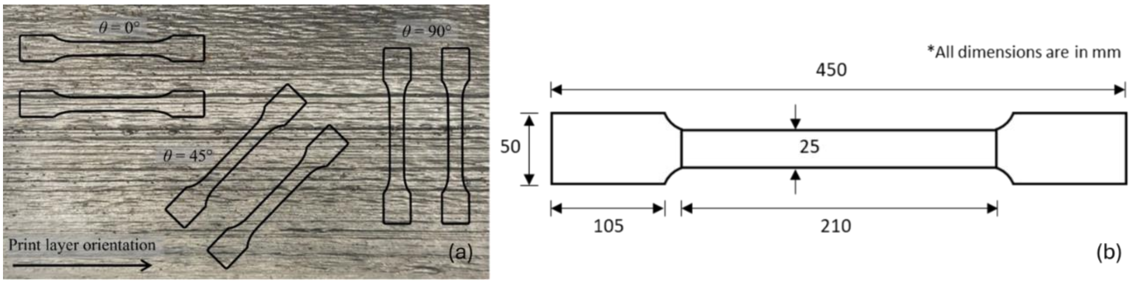

Figure (3): (a) Tensile coupon orientation relative to printing direction (Kyvelou et al., 2020), and (b) Dimensions of the tensile coupons

Numerical Modeling for Specimen Printed at 90 Degrees (Tension)

To model the AM'd specimen on ABAQUS, the specimen was divided into 90 layers along the 450mm long direction, connected by interactions. Each layer's thickness was 5 mm. The coupon specimens' dimensions are illustrated in Fig. 3(b). A mesh size of 1.0x1.0 mm and C3D8R solid elements (8-node linear-brick elements with reduced integration) was used.

Material Properties

The tensile test was experimentally performed on an AM'd specimen made of Grade 308LSi austenitic stainless-steel wires. Firstly, the modulus of elasticity and Poisson's ratio were taken as 118,400 MPa and 0.3, respectively. The Ramberg-Osgood material model was adopted, where the yield and ultimate stresses were obtained in accordance with (Kyvelou et al., 2020). In addition, density was defined as 7.85×10^{-9} ton/mm^3, thermal conductivity was 15.2 w/mk for temperatures between 0 and 100ºC, while it was taken as 28 w/mk at 1400ºC, specific heat was 450 j/kg K, and expansion coefficient was taken as 17.3 µm/mºC for the 308Lsi stainless-steel material, which had to be defined due to the presence of temperature variation. Moreover, ductile damage was defined to predict the initiation of damage due to coalescence in ductile material. For cases of uniaxial stress, the von-Mises stress is equal to the applied uniaxial stress, where stress triaxiality is equal to one third the summation of applied stresses divided by the von-Mises stresses, and the stress triaxiality is reduced to 1/3 for cases of uniaxial stress. Finally, the strain rate is assumed 0 for quasi-static analysis and the fracture strain was taken as 0.35, in accordance with Kyvelou et al. (2020).

Step Definition

An initial step was inserted by default in the module, where boundary conditions, interactions, pre-defined fields could be set up at the beginning of the analysis. Elevated temperatures of deposited steel materials during the printing process can cause internal residual stresses. Accordingly, the nodal displacements that take place during the process can be simulated using transient coupled temperature-displacement steps. The coupled-temperature displacement-step type allows the solver to consider the temperature degrees of freedom (DOF) along with displacements during the analysis. The initial and maximum increment sizes were taken as 0.1 and 1, respectively, while the step size was not kept constant and varied by the solver depending on the convergence of the solution. For the whole model to be simulated, 92 steps were used including the initial step and final step related to the tensile-test loading. The rest of steps were concerning the interactions, boundary conditions, and pre-defined fields between consecutive layers.

Interactions

The numerical-simulation approach of the printing process adopted in this work follows the element-death and- rebirth technique, which was widely adopted by previous researchers (Ding et al., 2011; Chiumenti et al., 2010; Xiong et al., 2017; Tröger et al., 2024), using *Model Change from the interaction module in ABAQUS. This approach follows that only the elements of the deposited material are active, while the rest of the elements in the model are deactivated. Surface-to-surface contact (standard) interaction was used, which described the contact between two deformable surfaces or between a deformable surface and a rigid surface. Fig. 4(a) shows an example of an interaction which took place between the layers (highlighted in red colour). In this simulation, surface-to-surface interaction between each two contiguous layers, at its creation step, was defined. All the interactions' definitions were automated using Python code, as the logic of the script is illustrated in Fig. (5) and a sample of the code is provided in the appendix. Python scripting in ABAQUS provides a time efficient alternative to manual definition of the interactions between successive layers.

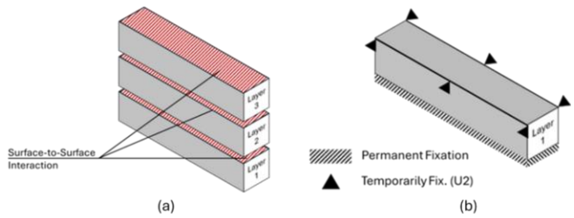

Figure (4): Interaction definition between successive layers for the 90-degree specimen and (b) Layer movement constraints in the vertical direction

Boundary Conditions

Fig. 4 (b) shows the boundary conditions for the first layer during the corresponding printing step. To limit convergence issues, the surface of each layer is constrained in the vertical (U2) direction at the initiation of the printing step, then deactivated afterwards. This approach showed limited discrepancies when compared to non-constrained interlayer surfaces, while avoiding any convergence errors from the solver.

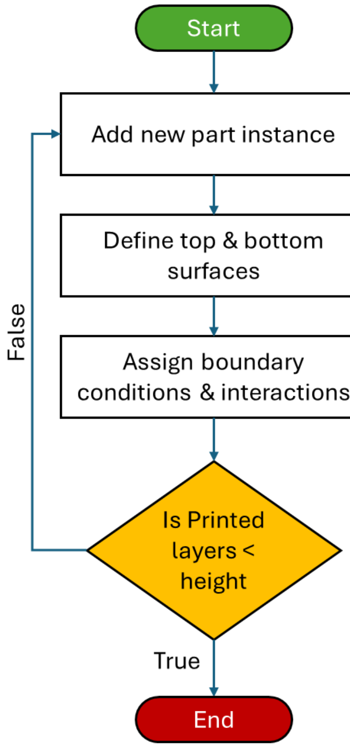

Figure (5): A flowchart describing the logic of the Python script

Pre-defined Fields and Amplitude Definitions

Ninety pre-defined fields were needed to be defined in the analysis. Each layer in the simulation was activated with an initial temperature equal to 1400°C (Ding et al., 2011). Consequently, the temperature of the layer was lowered until reaching the cooling temperature (< 30°C). To simulate the temperature decay for the layers, amplitudes were defined. The amplitude curve is a tool used for allowing variations of temperature using step time or total time.

Application of Tensile Load

A displacement controlled tensile test was simulated for the specimen. In this simulation, the load was applied on the middle of the surface on the longitudinal direction of the specimen. Thus, a reference point was inserted in the middle of the top layer, connected to the surface using a kinematic coupling constraint, allowing relative displacements between the coupled nodes on the surface. Subsequently, a 1x1 mm mesh size was defined, following the practices of Xiong et al. (2017), without compromising the computational efficiency.

Both FEMs for specimens printed at 45 degrees and 0 degree were created using the same procedures as in the 90- degree specimen. The 90-degree specimen was sketched as layers transversal to the printing direction, the 45-degree specimen was sketched as slanted layers with 45 degrees to the printing direction, and the 0-degree specimen was sketched as layers parallel to the printing direction. Moreover, there were differences in the material properties for each specimen. For the 45-degree specimen, the Young's modulus, and Poisson's ratio were taken as 193,600 MPa and 0.3, respectively. For the 0-degree specimen, the Young's modulus, and Poisson's ratio were taken as 132,400 MPa and 0.3, respectively (Kyvelou et al., 2020).

Tension Simulation Results and Discussion

90-degree Oriented Specimen Results

Two simulations were performed on specimen AB-8-90-B2 provided by Kyvelou et al. (2020) in experimental testing. The first FE model considered the simulation of the 3D printed specimen as layers connected by interactions to simulate the 3D printing process. The second model considered the specimen to be simulated as one part only. The specimen was simulated with orientation of 90 degrees to the printing direction. Fig. (6) displays the stress distribution along the specimen with failure location in the experimental testing. As shown, the failure of the first FE model occurred at nearly one-third of the specimen height. This mode of failure was contiguous to the failure of the experimental testing shown in Fig. 6 (a). On the other hand, the failure of the second model was in the middle. Moreover, Fig. (7) shows the stress-strain curve of the simulation models and the experimental work in (Kyvelou et al., 2020). It can be noticed that the second FE-model curve slightly deviated from the experimental one. However, the first FE-model behaved the same as in the experiment. The results proved the importance of simulating the 3D printed elements as layers in ABAQUS. Moreover, the first model exhibited the same elastic deformation and had the same yield point as in the experiment. Also, it could be obtained from the simulation results that the maximum stress capacity of the specimen was 478.8 MPa, while the maximum stress capacity of the experimental testing was 479 MPa. Thus, a difference of 0.04 % was recorded.

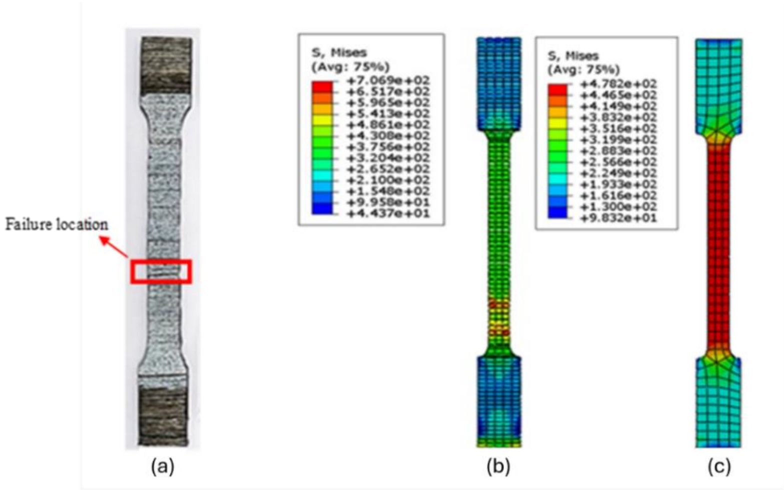

Figure (6): (a) Failure mode of 90-degree oriented specimen of the experimental testing (Kyvelou et al., 2020), (b) Stress distribution along the 90-degree specimen using layers' approach (this study), and (c) Stress distribution along the 90-degree specimen modeled as one part (this study)

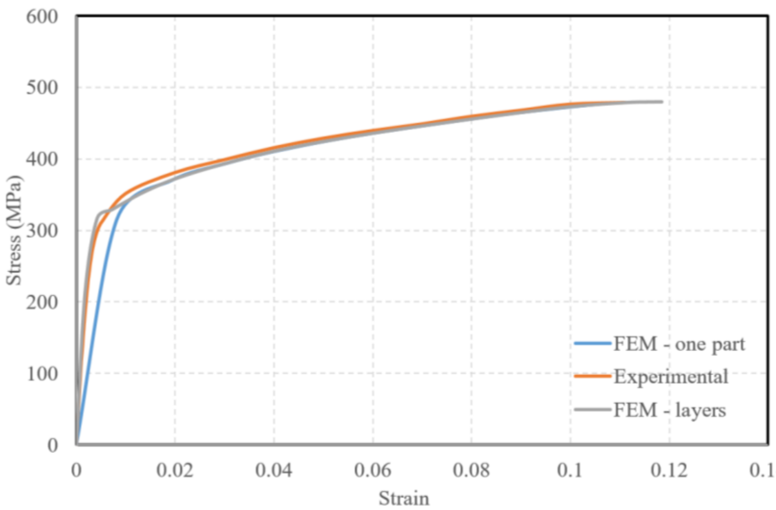

Figure (7): Stress-strain relation for 90-degree printed specimen

45-degree and 0-degree Oriented Specimens' Results

The simulation was performed on both specimen AB-8-45-D3 and specimen AB-8.0-0°-A2 from the experimental testing (Kyvelou et al., 2020). For the 45-degree model of specimen A, failure occurred at nearly one-third of the specimen, and the failure mode from the simulation aligned with the experimental testing. Similarly, for specimen AB-8.0-0°-A2, which was oriented parallel to the printing direction, failure took place near the middle, as shown in Fig. (8). In both cases, stress-strain curves were produced and compared to those from the experiments, as depicted in Fig. (9). For specimen AB-8-45-D3, a 2.4% discrepancy was observed in the yielding stress between the two curves, with the maximum tensile-stress capacity of the experimental test at 592 MPa and that of the simulation at 599 MPa, resulting in a 1.18% difference in ultimate tensile stress. For specimen AB-8.0-0°-A2, the yielding state showed a small 3.5% discrepancy, with a maximum recorded stress of 514 MPa from the experiment and 520 MPa from the simulation, leading to a 1.17% difference in ultimate tensile stress.

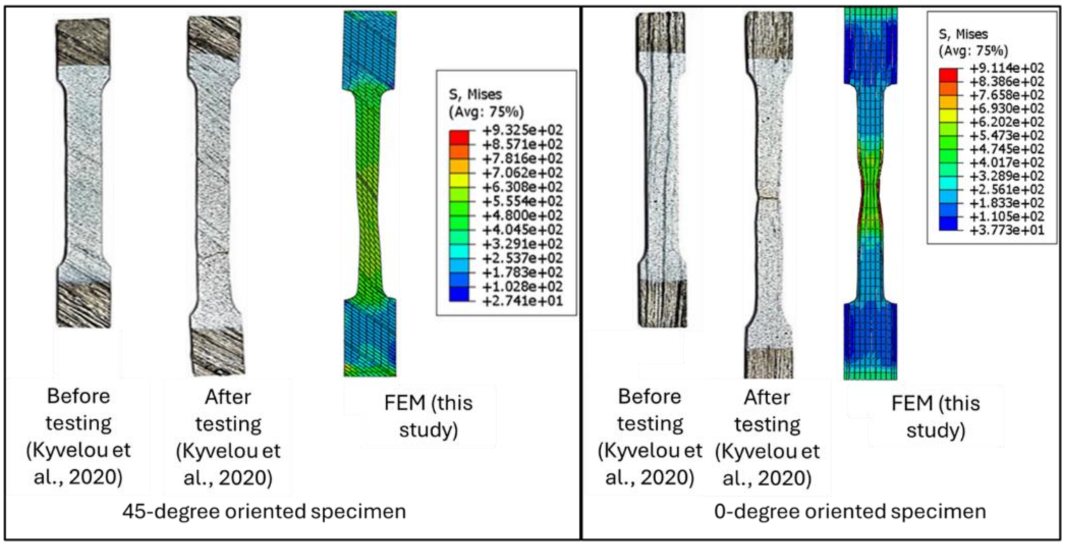

Figure (8): 45º and 0º tensile coupon specimens

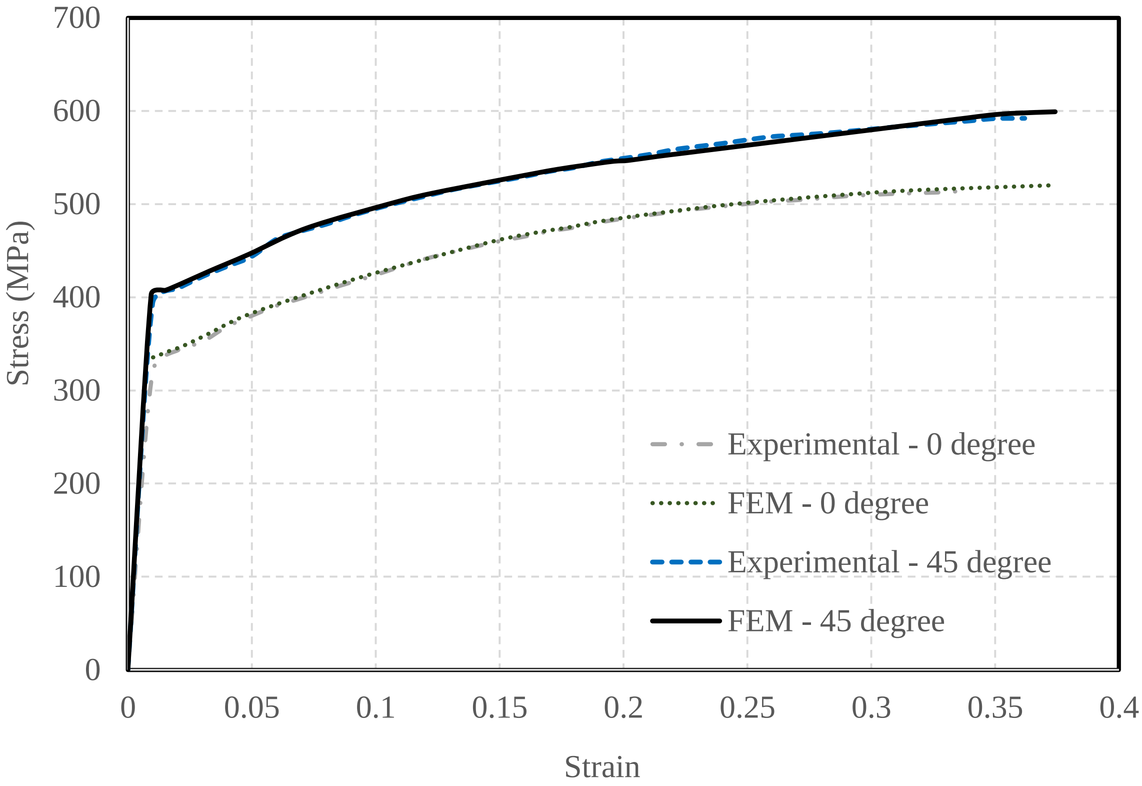

Figure (9): Stress-strain relation for 45-degree and 0-degree printed specimens

Numerical Modeling for Specimen Printed at 90 Degrees (In Compression)

The specimens used for the compression test conducted by Huang et al. (2022b) were circular hollow section columns. The specimen chosen for the numerical modeling was C105-3, the outer radius of which is 105 mm, and the thickness of which is 4.17 mm. The total height of the column is 850 mm. The column was divided into layers as performed in the tension simulation. Moreover, most of the material properties defined for the compression simulation were the same as in the tension simulation. However, for the CHS, the Young's modulus and Poisson's ratio were taken as 90200 MPa and 0.3, respectively. The simulation for the buckling test was different from the tension simulation in the step module in ABAQUS. For the CHS, a linear buckling analysis was performed to obtain the buckling modes of the part.

Step Module Definitions

For layer simulation, coupled-temperature displacement step type was used as in tension simulation. For the CHS specimen, 85 coupled-temperature displacement steps were defined. In addition, the loading step was defined as a buckle step in linear perturbation module. The numbers of requested eigenvalues and vectors per iteration have been adjusted based on the required number of eigenmodes.

Interaction Module Definitions

The interaction between column layers was surface-to-surface contact (standard) as defined for the tension simulation. The interactions tie constraints between the top surface of the part and the bottom surface of its successive part. Constraints of the type "Tie" between adjacent surfaces transfers the nodal temperatures and displacements from one surface to another. Moreover, two reference points were inserted at both column ends, as these points were the location of the applied loads. Consequently, rigid-body constraints were created between the surface and the reference bottom to be connected and work as one body.

Boundary Condition Module Definitions

At first, room-temperature boundary conditions were defined at the surfaces of all parts in the simulation. For the base part, the bottom was prevented from translation in X, Y, and Z directions and from rotational displacement about the longitudinal Z direction, while the top part was prevented from translation in X and Y directions only. Pre-defined temperature fields were defined for each part of the CHS column as defined for tension simulation, where the simulated deposited materials were assigned a temperature of 1400°C on deposition. Also, an appropriate meshing size of 30 mm was used for the tubular column.

Load Application for the Linear Simulation

The load was applied to the reference point at the top of the column. Temporarily, the load value was inserted as -1. After getting the eigenvalue at the end of linear buckling analysis, the critical load would be the eigenvalue multiplied by -1. The negative sign was considered for direction only.

Then, adjust the "Edit keywords" in the linear model by writing * NODE FILE U at the end after the output field. This would import the displacement values for the non-linear buckling analysis. Also, the accuracy of the results was maintained after running the linear model, the eigenvalue was obtained to be 1.076×10^{7} N.

Step Module for the Non-linear Simulation

The loading step was replaced by general non-linear static Riks. The static Riks analysis method in ABAQUS is a numerical technique used to solve non-linear equilibrium problems, particularly for tracing the post-buckling response of structural elements, where traditional methods may fail. The initial increment size was 0.01 and the maximum increment size was 1. The point load was changed to -1.076×10^{7}N, which was the eigenvalue of the linear simulation. The non-linear model was adjusted through "Edit keywords" by adding "IMPERFECTION, FILE = Linear, STEP = 1" just before the step.

The buckling load was calculated by the multiplication of the eigenvalue and the Load Proportionality Factor (LPF) to be 7.01×10^{5} MPa and the reaction force obtained from the analysis was 6.95×10^{5} MPa. There was a 0.9 % difference between the values resulting from the numerical model and those resulting from experimenting.

90-degree Oriented Specimen Results (Compression)

Fig. (10) displays the stress distribution along the tubular column. It could be observed that the deformation of the tubular column in the simulation was consistent to the deformation in the experimental testing. The stress-strain relationships are plotted in Fig. (11). It could be noticed that both curves were in good agreement before reaching the ultimate stress, while the post-peak behavior of the specimen differed from the numerical model. This can be attributed to the idealized representation of the support conditions in the numerical model compared to the physical test, and the assumption of perfect bonding between layers, which can contribute to discrepancies when compared to experimental behavior, where imperfections at layer interfaces are present.

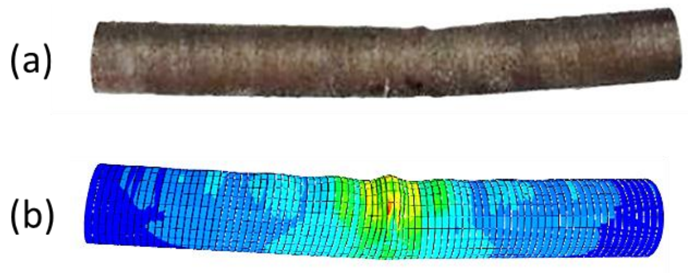

Figure (10): (a) Failure mode of the experimental testing of the CHS column (Huang et al., 2022b) and (b) Stress distribution and failure mode along the CHS column (this study)

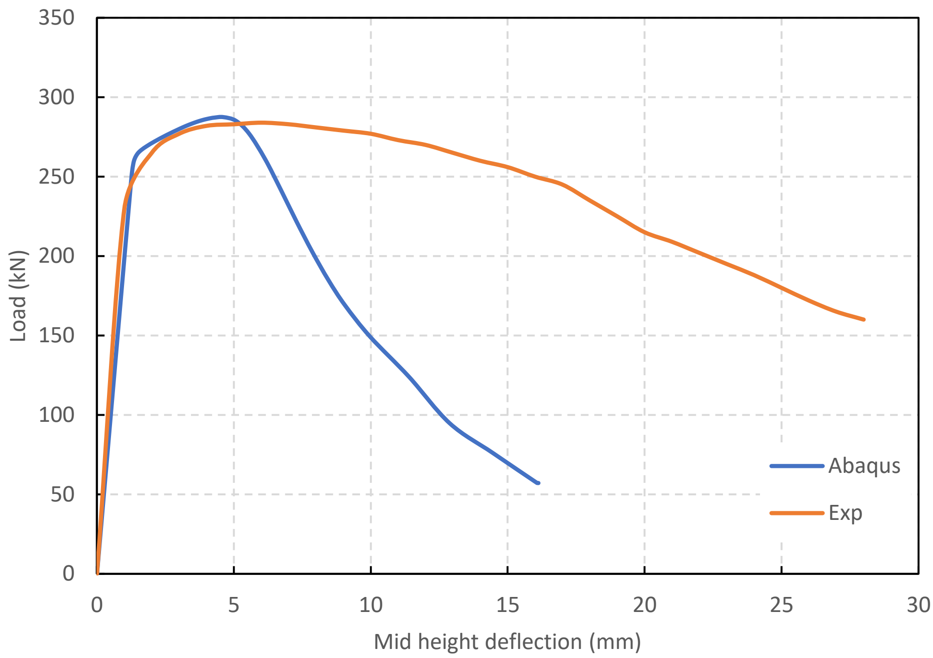

Figure (11): Load vs. mid-height deflection curve for 90-degree printed circular hollow section column

SUMMARY AND CONCLUSIONS

In this research, detailed procedures for creating numerical models of AM'd specimens were presented. Three models have been developed for tension-test simulation. Each model represented a specific printing orientation (0, 45, and 90 degrees). The specimen used for tension was a dog-bone specimen the dimensions of which were taken according to ISO standards. On the other hand, one model has been developed for compression simulation. The specimen used for compression was a CHS column printed in vertical direction (90 degrees). Most of simulation procedures were the same for all models, such as interactions, step-type, pre-defined fields, specific heat, conductivity, expansion coefficient, and fracture characteristics. However, the differences lie on the boundary conditions for each simulation, as each test required a different displacement control at both ends of the specimen. Also, the elastic and plastic properties have been changed for each model due to material anisotropy.

Based on the work conducted in this research, the following conclusions were drawn:

- The adopted coupled-temperature displacement step proved effective in predicting the mechanical behavior of printed elements subjected to tensile load, considering the temperature variation.
- The material anisotropy strongly impacts the mechanical response of each printing orientation depending on the elastic and plastic properties of the specimen.
- Buckle and Riks steps represented the most efficient techniques for compression loading simulation and evaluation of the strength of the circular hollow section column.
- Interactions had to be inserted between successive layers for them to work as one object. Surface-to-surface contact (tie constraint) was properly working for the simulation and gave precise values to the experimental testing for both tensile and compressive loading.
- Temperature and amplitude fields must be pre-defined to simulate the drop in temperature until reaching the cooling temperature.

As the scope of this work is limited by the scale of the specimens and utilizing a layer-by-layer approach, future work can include more large-scale modeling of the additive manufacturing processes, while adopting other approaches that can capture the printing speed and direction more precisely. In addition, a study of the discrepancies in different element types (i.e., Eulerian *vs.* Lagrangian) can be included in these models. Large-scale models will require automation of part partitioning (slicing), definitions of material orientation, interactions between layers and boundary conditions, making the Python scripting approaches invaluable.

Appendix

Script 1. Sample of the Python script used for automating interaction definitions

```
model = mdb.models[‘Model-90’]
model.ContactProperty(‘IntProp-1’)
model.interactionProperties[‘IntProp-1’].CohesiveBehavior()
a = model.rootAssembly
for i in range(1,90):
    region1=a.surfaces[‘Surf-‘+str(i)+’-up’]
    region2 = a.surfaces[‘Surf-‘+str(i+1)+’-bottom’]
    model.SurfaceToSurfaceContactStd(name=’Int-‘+str(i),
        createStepName=’Step-‘+str(i), main=region1, secondary=region2,
        sliding=SMALL, thickness = ON, interactionProperty=’IntProp-1’,
        adjustMethod=NONE, initialClearance=OMIT, datumAxis=None,
        clearanceRegion=None)
```

REFERENCES

ABAQUS. (2019). “Version 2019. Pawtucket, USA”. Hibbitt, Karlsson & Sorensen, Inc.

Abusalma, H., Eisazadeh, H., Hejripour, F., Bunn, J., and Aidun, D.K. (2022). “Parametric study of residual stress formation in wire and arc additive manufacturing”. Journal of Manufacturing Processes, 75, 863-876. https://doi.org/10.1016/j.jmapro.2022.01.043

Ayan, Y., and Kahraman, N. (2022). “Bending fatigue properties of structural steel fabricated through wire arc additive manufacturing (WAAM)”. Engineering Science and Technology: An International Journal, 35, 101247. https://doi.org/10.1016/j.jestch.2022.101247

Barakat, S., Alhalabi, M., Mostafa, O., and Fattouh, I.H. (2022). “Size optimization of truss structures using calibrated shuffled complex evolution algorithm”. Jordan Journal of Civil Engineering. 16 (4), 540-548.

Calignano, F., Manfredi, D., Ambrosio, E.P., Biamino, S., Lombardi, M., Atzeni, E., ..., and Fino, P. (2017). "Overview on additive manufacturing technologies". Proceedings of the IEEE, 105(4), 593-612. https://doi.org/10.1109/JPROC.2016.2625098

Chiumenti, M., Cervera, M., Salmi, A., De Saracibar, C. A., Dialami, N., and Matsui, K. (2010). "Finite element modeling of multi-pass welding and shaped metal deposition processes". Computer Methods in Applied Mechanics and Engineering, 199 (37-40), 2343-2359. https://doi.org/10.1016/j.cma.2010.02.018

Ding, J., Colegrove, P., Mehnen, J., Ganguly, S., Almeida, P. S., Wang, F., and Williams, S. (2011). "Thermo-mechanical analysis of wire and arc additive layer manufacturing process on large multi-layer parts". Computational Materials Science, 50 (12), 3315-3322. https://doi.org/10.1016/j.commatsci.2011.06.023

Feucht, T., Lange, J., and Erven, M. (2019). "3-D-printing with steel: Additive manufacturing of connection elements and beam reinforcements". CE/Papers, 3 (3-4), 343-348. https://doi.org/10.1002/cepa.1064

Feucht, T., Lange, J., Waldschmitt, B., Schudlich, A.K., Klein, M., and Oechsner, M. (2020). "Welding process for the additive manufacturing of cantilevered components with the WAAM". Advanced Joining Processes, 67-78. https://doi.org/10.1007/978-981-15-2957-3_5

Galeb, A.C., and Khayoon, A.M. (2013). Optimum design of transmission towers subjected to wind and earthquake loading". Jordan Journal of Civil Engineering, 7 (1), 70-92.

Gardner, L., Kyvelou, P., Herbert, G., and Buchanan, C. (2020). "Testing and initial verification of the world's first metal AM'd bridge". Journal of Constructional Steel Research, 172, 106233. https://doi.org/10.1016/j.jcsr.2020.106233

Guo, N., and Leu, M.C. (2013). "Additive-manufacturing: technology, applications and research needs". Frontiers of Mechanical Engineering, 8, 215-243.

Hadjipantelis, N., Weber, B., Buchanan, C., and Gardner, L. (2022). "Description of anisotropic material response of wire and arc additively manufactured thin-walled stainless steel elements". Thin-Walled Structures, 171, 108634. https://doi.org/10.1016/j.tws.2021.108634

Huang, C., Li, L., Pichler, N., Ghafoori, E., Susmel, L., and Gardner, L. (2023). "Fatigue testing and analysis of steel plates manufactured by wire-arc directed energy deposition". Additive Manufacturing, 103696. https://doi.org/10.1016/j.addma.2023.103696

Huang, C., Meng, X., and Gardner, L. (2022a). "Cross-sectional behavior of wire arc additively manufactured tubular beams". Engineering Structures, 272, 114922. https://doi.org/10.1016/j.engstruct.2022.114922

Huang, C., Meng, X., Buchanan, C., and Gardner, L. (2022b). "Flexural buckling of wire arc additively manufactured tubular columns". Journal of Structural Engineering, 148 (9), 04022139. https://doi.org/10.1061/(ASCE)ST.1943-541X.0003427

Kloft, H., Empelmann, M., Hack, N., Herrmann, E., and Lowke, D. (2020). "Reinforcement strategies for 3D-concrete-printing". Civil Engineering Design, 2 (4), 131-139.

Kořínek, M., Halama, R., Fojtík, F., Pagáč, M., Krček, J., Krzikalla, D., Kocich, R., and Kunčická, L. (2021). "Monotonic tension-torsion experiments and FE modeling on notched specimens produced by SLM technology from SS316L". Materials, 14 (1), 1-15. https://doi.org/10.3390/ma14010033

Kraus, M., Winkler, P., Hammer, S., Reimann, J., Hildebrand, J., and Bergmann, J. P. (2022). "Geometric imperfections of additive manufactured members". Engineering Structures, 252, 113596. https://doi.org/10.1016/j.engstruct.2021.113596

Kyvelou, P., Slack, H., Mountanou, D. D., Wadee, M. A., Britton, T. Ben, Buchanan, C., and Gardner, L. (2020). "Mechanical and micro-structural testing of wire and arc additively manufactured sheet material". Materials and Design. 192, 108675. https://doi.org/10.1016/j.matdes.2020.108675

Laghi, V. (2021). "Study of innovative steel 3D-printed process for structural engineering application". Dissertation, University of Bologna. DOI.10.48676/unibo/amsdottorato/9726

Laghi, V., Palermo, M., Gasparini, G., Girelli, V. A., and Trombetti, T. (2020a). "Experimental results for structural design of wire-and-arc additive manufactured stainless steel members". Journal of Constructional Steel Research, 167, 105858. https://doi.org/10.1016/j.jcsr.2019.105858

Laghi, V., Palermo, M., Gasparini, G., Girelli, V. A., and Trombetti, T. (2021). "On the influence of the geometrical irregularities in the mechanical response of wire-and-arc additively manufactured planar elements". Journal of Constructional Steel Research, 178, 106490. https://doi.org/10.1016/j.jcsr.2020.106490

Laghi, V., Palermo, M., Gasparini, G., Veljkovic, M., and Trombetti, T. (2020b). "Assessment of design mechanical parameters and partial safety factors for wire-and-arc additive manufactured stainless steel". Engineering Structures, 225, 111314. https://doi.org/10.1016/j.engstruct.2020.111314

Laghi, V., Palermo, M., Tonelli, L., Gasparini, G., Girelli, V. A., Ceschini, L., and Trombetti, T. (2022). "Mechanical response of dot-by-dot wire-and-arc additively manufactured 304L stainless steel bars under tensile loading". Construction and Building Materials, 318, 125925. https://doi.org/10.1016/j.conbuildmat.2021.125925

Mechtcherine, V., Buswell, R., Kloft, H., Bos, F. P., Hack, N., Wolfs, R., ..., and Neef, T. (2021). "Integrating reinforcement in digital fabrication with concrete: A review and classification framework". Cement and Concrete Composites, 119, 103964. https://doi.org/10.1016/j.cemconcomp.2021.103964

Megahed, M., Mindt, H. W., N'Dri, N., Duan, H., and Desmaison, O. (2016). "Metal additive-manufacturing process and residual stress modeling". Integrating Materials and Manufacturing Innovation, 52016. https://doi.org/10.1186/s40192-016-0047-2

Müller, J., Grabowski, M., Müller, C., Hensel, J., Unglaub, J., Thiele, K., ..., and Dilger, K. (2019). "Design and parameter identification of wire and arc additively manufactured (WAAM) steel bars for use in construction". Metals, 9 (7), 725. https://doi.org/10.3390/met9070725

Rosli, N.A., Alkahari, M.R., bin Abdollah, M.F., Maidin, S., Ramli, F.R., and Herawan, S.G. (2021). "Review on effect of heat input for wire arc additive manufacturing process". Journal of Materials Research and Technology, 11, 2127-2145. https://doi.org/10.1016/j.jmrt.2021.02.002

Saleh, Y.N., Mourad, S.A., and Ibrahim, A.M. (2024, August). "Topology optimization of vertical shear links in eccentrically braced frames". In: Structures (66, 106821). Elsevier. https://doi.org/10.1016/j.istruc.2024.106821

Sequeira Almeida, P.M. (2012). "Process control and development in wire and arc additive manufacturing". Doctoral Dissertation, Cranfield University. https://dspace.lib.cranfield.ac.uk-/handle/1826/7845

Silvestru, V.-A., Ariza, I., and Taras, A. (2022). "Ductility and buckling behavior of point-by-point wire arc additively manufactured steel bars". ce/papers, 5 (4), 226-234. https://doi.org/10.1002/cepa

Singh, S., Ramakrishna, S., and Singh, R. (2017). "Material issues in additive manufacturing: A review". Journal of Manufacturing Processes, 25, 185-200. https://doi.org/10.1016/j.jmapro.-2016.11.006

Tröger, J. A., Hartmann, S., Treutler, K., Potschka, A., and Wesling, V. (2024). "Simulation-based process parameter optimization for wire arc additive manufacturing". Progress in Additive Manufacturing, 1-14. https://doi.org/10.1007/s40964-024-00597-x

van Bolderen, G. (2017). "Exploration of stability of 3D-printed steel members: A study to buckling behaviour of wire and arc additively manufactured stainless steel tubular columns". http://resolver.tudelft.nl/uuid:cf099386-6a89-44f6-849c-0738177e7ea1

Xiong, J., Lei, Y., and Li, R. (2017). "Finite element analysis and experimental validation of thermal behavior for thin-walled parts in GMAW-based additive manufacturing with various substrate preheating temperatures". Applied Thermal Engineering, 126, 43-52.

Zhang, R., Gardner, L., Buchanan, C., Matilainen, V.P., Piili, H., and Salminen, A. (2021). "Testing and analysis of additively manufactured stainless steel CHS in compression". Thin-Walled Structures, 159, 107270. https://doi.org/10.1016/j.tws.2020.107270

Zhang, R., Gardner, L., Amraei, M., Buchanan, C., and Piili, H. (2023). "Testing and analysis of additively manufactured stainless steel corrugated cylindrical shells in compression". Journal of Engineering Mechanics, 149 (4), 04023013.